Article

Applied Spectroscopy

Applied Spectroscopy
2019, Vol. 73(7) 767–773

DOI: 10.1177/0003702819842558
journals.sagepub.com/home/asp
SAGE

Identification of Large Isotope Anomalies in Quartz by Infrared Spectroscopy

Ryan C. Ogliore[1], Cosette Dwyer[2], Michael J. Krawczynski[3], Hélène Couvy[3], Max Eisele[4], and Justin Filiberto[5]

Abstract

We report an infrared (IR) spectroscopic technique to detect quartz grains with large isotope anomalies. We synthesized isotopically doped quartz and used Fourier transform infrared spectroscopy (FT-IR) in two different instruments: a traditional far-field instrument and a neaSpec nanoFT-IR, to quantify the shift in the peak of the Si–O stretch near 780 cm^{-1} as a function of isotope composition, and the uncertainty in this shift. From these measurements, we estimated the minimum detectable isotope anomaly using FT-IR. The described technique can be used to nondestructively detect very small (30 nm) presolar grains. In particular, supernova grains, which can have very large isotope anomalies, are detectable by this method.

Keywords

Fourier transform infrared, FT-IR, infrared spectoscopy, near-field infrared spectoscopy, quartz, isotope anomalies, presolar grains

Date received: 17 October 2018; accepted: 30 December 2018

Introduction

Presolar grains are small particles (mostly $< 10\,\mu m$) that formed in the outflows of other stars in the galaxy and are found at the 1–100 parts-per-million (ppm) level in the matrix of primitive meteorites, interplanetary dust particles, and samples returned from primitive solar system bodies.[1] They can be crystalline or amorphous[2] and are identified by their large isotope anomalies, often tens of percent different from isotope ratios in grains that formed in the solar system. Presolar grains are either identified after chemical separation from their host rock (e.g., Amari et al.[3]) or by in-situ analysis of, for example, a polished meteorite section (e.g., Floss and Stadermann[4]). Traditionally, isotope anomalies in individual grains $<10\,\mu m$ in size are identified by secondary-ion mass spectrometry (SIMS), a destructive technique. Analyses by SIMS can amorphize crystalline phases and leave the presolar grain too damaged for meaningful follow-up analyses by transmission electron microscopy of the grain's structure and elemental composition. Nondestructive identification of presolar grains with large isotope anomalies would allow for more detailed subsequent structural analyses of these grains to constrain their formation environment.[5] Liu et al.[6] describe a nondestructive technique to identify a particular subgroup of presolar silicon carbide grains of relatively large sizes. Here we describe a technique to identify isotopically anomalous presolar grains, many of which are $<1\,\mu m$ in size, using infrared (IR) spectroscopy.

Isotope substitutions in a crystal can alter that crystal's vibrational modes (e.g., Sato and McMillan[7]). These vibrational modes are probed by vibrational spectroscopy techniques such as Raman and IR spectroscopy. Meteorites containing isotopically anomalous presolar grains are traditionally prepared as 30 μm-thick thin sections mounted on a glass slide with epoxy. The nature of the meteorite sample (many grains are optically opaque) necessitates the use of reflected-light spectroscopy rather than transmitted-light spectroscopy.

Here we demonstrate the use of reflected-light IR spectroscopy to identify isotope anomalies in quartz (SiO_2). We chose to investigate quartz because of its simple crystal

[1]Department of Physics, Washington University in St. Louis, St. Louis, MO, USA
[2]W. M. Keck Science Department, Scripps College, Claremont, CA, USA
[3]Department of Earth & Planetary Sciences, Washington University in St. Louis, St. Louis, MO, USA
[4]NeaSpec, Germany
[5]Lunar and Planetary Institute, USRA, Houston, TX, USA

Corresponding author:
Ryan C. Ogliore, 1 Brookings Drive, Physics Department, CB1105, Saint Louis, MO 63130-4862, USA.
Email: rogliore@physics.wustl.edu

structure, ease of experimental synthesis, and the recent discovery of supernova silica in meteorites[8] and supernova remnants.[9] We also demonstrate the use of near-field IR spectroscopy to identify large isotope anomalies in crystals as small as 50 nm in size.

Experimental Methods

The goal of this study is to determine the minimum detectable Si isotope anomaly in quartz from isotope-induced shifts in its IR reflectance spectrum. To this end, we synthesized quartz with three distinct isotope ratios using a piston cylinder apparatus at the Experimental Studies of Planetary Materials lab at Washington University in St. Louis. The pressure cell assembly is similar to that of Krawczynski and Grove[10] with the exception of the capsule design described below. The three types of synthesized quartz were: (1) quartz of terrestrial isotopic composition using normal amorphous silica powder; (2) quartz of nearly pure ^{30}Si; and (3) quartz of nearly pure ^{28}Si. The Si isotope ratios of these three samples are given in Table I. Three different quartz samples were synthesized from silica powders with normal terrestrial composition, 99.8% pure ^{28}Si silica powder (Cambridge Isotope Laboratories: Catalog Number SILM-3582), and 96.5% pure ^{30}Si silica powder (Cambridge Isotope Laboratories: Catalog Number SILM-4517). To ensure that the doped and undoped quartz crystals were synthesized at identical conditions, we created an experimental graphite capsule with two cylindrical holes to hold isotopically doped and undoped silica powders simultaneously without mixing (Fig. 1).

Table I. Si isotope ratios for the three synthesized quartz samples.

Ratio	Terrestrial quartz	^{28}Si quartz	^{30}Si quartz
^{29}Si/^{28}Si	5.1×10^{-2}	9.4×10^{-5}	5.1×10^{-2}
^{30}Si/^{28}Si	3.4×10^{-2}	6.2×10^{-5}	3.0×10^{1}

Each capsule with terrestrial and isotopically doped silica powders was heated in a 150 ton piston cylinder at a temperature of 1200 °C and a pressure of 1 GPa for 24 h. Under this temperature and pressure, β-quartz is synthesized.[11] The experimental charge was quenched, which resulted in a transition of β-quartz to α-quartz.[11] Grain sizes of the synthetic quartz were in the range of 20–100 μm (Fig. 1).

Each of the two capsules (terrestrial and ^{28}Si quartz, terrestrial and ^{30}Si quartz) was mounted in an Al annulus with epoxy along with natural quartz and olivine, and then polished. The terrestrial and ^{30}Si quartz capsule is shown in its Al annulus mount in Fig. 1.

Analytical Methods

We acquired IR reflectance spectra of the terrestrial, ^{28}Si, and ^{30}Si quartz by both traditional far-field micro-reflectance FT-IR and by near-field FT-IR.[12,13] The spatial resolution of the far-field micro reflectance FT-IR is diffraction limited; the spatial resolution of the near-field FT-IR is determined by the size of the metalized tip that is illuminated with a broadband IR laser beam. This tip, similar to that used in atomic-force microscopy, can be as small as ~30 nm.

The far-field IR reflectance spectra were acquired with a Nicolet iS50 FT-IR spectrometer (with a Nicolet continuum

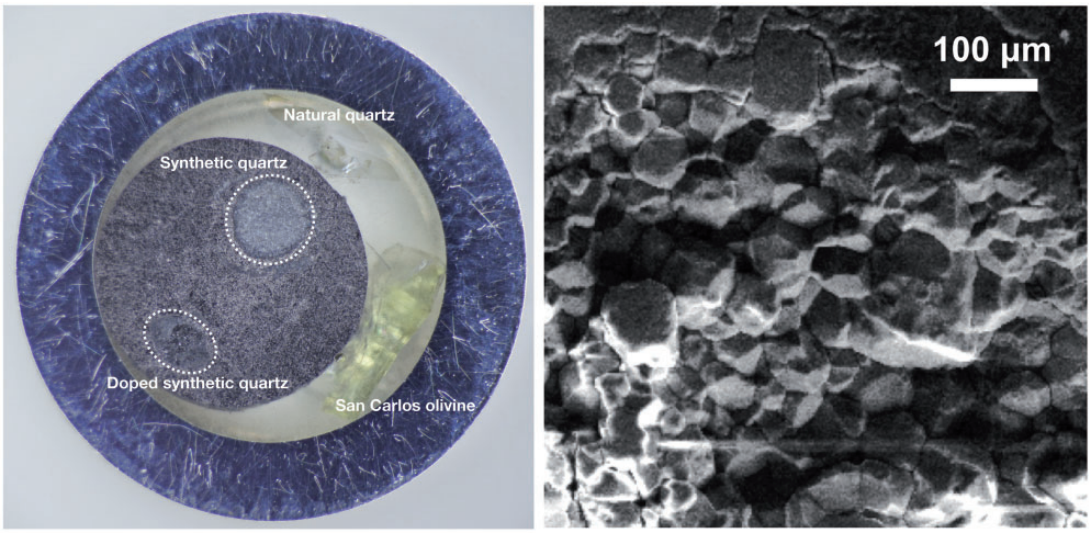

Figure 1. Left: Experimental capsule of terrestrial and ^{30}Si quartz mounted in epoxy in a 1 cm outer-diameter Al annulus, with natural quartz and terrestrial olivine to serve as standards. Right: Secondary electron image of synthesized ^{28}Si quartz showing grain sizes in the range of 20–100 μm.

microscope attachment) at Southern Illinois University, Carbondale. The spectral resolution was 0.5 cm^{-1} over a range of 500–1500 cm^{-1} and each spectrum was collected for ~10 min. Near-field IR spectra were acquired with a NeaSpec nanoFT-IR at a spectral resolution of 1 cm^{-1} over a range of 700–1500 cm^{-1} and were also collected for ~10 min.

Results

Strong peaks in both the far-field and near-field reflectance spectra were observed around 780 cm^{-1} and 1160 cm^{-1} (Figs. 3 and 4). The mode near 780 cm^{-1} is associated with asymmetric stretching vibrations of silicon against its tetrahedral oxygen "cage" (Fig. 2) and the mode near 1160 cm^{-1} is associated with an asymmetric Si–O stretching motion within the Si–O–Si linkages of α-quartz.[14]

For the far-field spectra, we could identify the wavenumber of the steepest slope near the absorbance peaks more precisely than the wavenumber of the absorbance peaks themselves, which could be relatively broad. We calculated numerical derivatives of the far-field spectra using a Savitzky–Golay filter[15] in Matlab to identify the wavenumber associated with the minimum slope. Uncertainties of these values were calculated as the standard deviation of repeated measurements of different crystals in the same synthesized sample, typically five for each sample.

Near-field amplitude spectra had a pre-edge bump near the 780 cm^{-1} wavenumber feature which made the estimation of the steepest slope imprecise. The NeaSpec nanoFT-IR also (indirectly) measures the real component of the refractive index of the sample, the phase (Fig. 4). The phase spectra lacked this variable pre-edge bump and yielded a more precise estimate of the position of the steepest slope, so the phase spectra were used instead of the amplitude spectra to estimate the position of this peak. Similar to the far-field spectra, we calculated numerical derivatives via a Savitzky–Golay filter and estimated the standard deviation from repeated measurements of different crystals of the same synthesized samples.

The synthesized quartz of terrestrial Si isotope composition had a peak that was consistently 18 cm^{-1} higher than the ^{30}Si-doped quartz for the ~780 cm^{-1} Si–O stretch (Fig. 3). The 1160 cm^{-1} feature in synthesized terrestrial-composition quartz was 7–12 cm^{-1} higher than the ^{30}Si quartz, but variable in its position (possibly due to crystal orientation and size). The ^{28}Si-doped quartz had a peak about 1 cm^{-1} higher than the terrestrial quartz for the ~780 cm^{-1} Si–O stretch. A natural quartz crystal was measured to have a spectrum nearly identical to the synthesized quartz of terrestrial Si isotope composition. The mean value of the peaks of these features for multiple scans is shown in Table II.

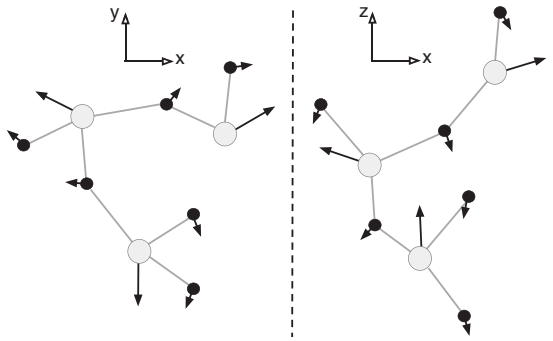

Figure 2. Displacement patterns for the mode associated with the 780 cm^{-1} feature. Dark circles are oxygen, lighter circles are silicon. Reproduced from Sato and McMillan.[7]

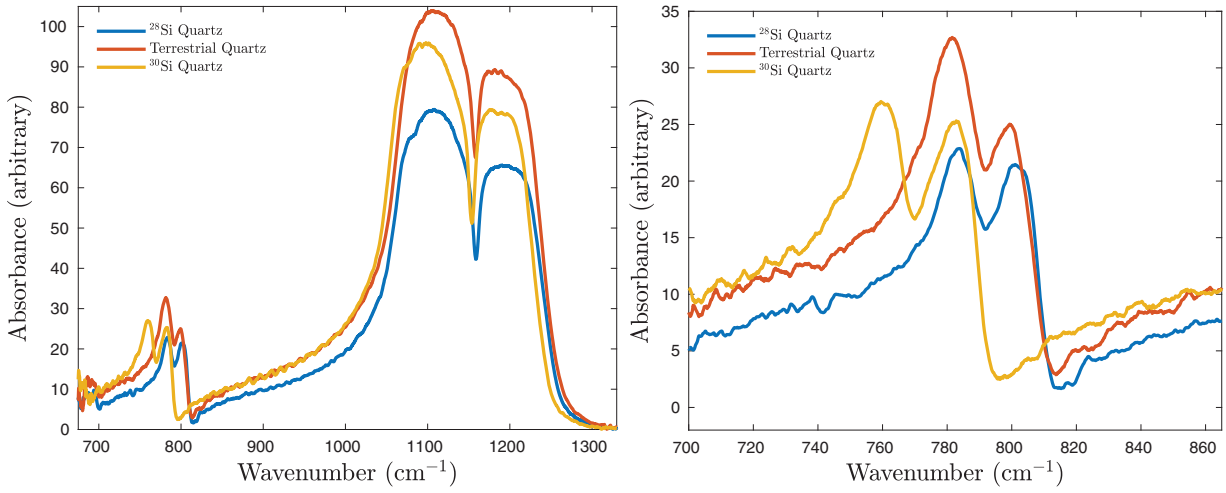

Figure 3. Left: Representative far-field IR reflectance spectra of synthetic quartz grains using a Nicolet iS50 FT-IR. Right: Detailed view of peaks around 780 cm^{-1}.

The nanoFT-IR spectra of ^{30}Si quartz showed a 780 cm^{-1} feature that was consistently 16 cm^{-1} lower than this feature in the spectra of terrestrial-composition quartz. The large feature around 1100 cm^{-1} in the amplitude spectra (Fig. 4) also shifted with isotope composition but was more variable (similar to the far-field spectra). The mean value of the ~780 cm^{-1} Si–O stretch in the ^{28}Si-doped quartz was at a higher wavenumber than the terrestrial-composition quartz, but the uncertainties (the variability in repeated measurements of each sample) overlap. Natural quartz was measured to have a spectrum nearly identical to that of the synthesized quartz of terrestrial Si isotope composition. Mean values of the position of 780 cm^{-1} feature for the nanoFT-IR spectra are also given in Table II.

Table II. Mean values of the location of 780 cm^{-1} feature for far-field FT-IR and nanoFT-IR.

Sample	Far-field FT-IR (cm^{-1})	NanoFT-IR (cm^{-1})
^{28}Si-enriched quartz	807.4	799.9
Undoped quartz	806.5	799.1
Natural quartz	806.4	798.7
^{30}Si quartz	788.2	782.5

Discussion

Sato and McMillan[7] measured the ~780 cm^{-1} Si–O stretch feature to be 21 cm^{-1} lower in the transmission far-field spectra of powdered ^{30}Si quartz than in terrestrial quartz. This shift is about 3 cm^{-1} larger than the shift we measured in our reflectance spectra of similar samples (Sato and McMillan[7] did not measure ^{28}Si quartz). The different shifts are likely due to transmission versus reflectance spectra, which sample different proportions of the absorption and reflection components, resulting in different peak shapes and positions.[16,17]

The vibrational modes in quartz as a function of the crystal's Si isotopic composition can be calculated numerically using the density functional perturbation theory. We calculated vibrational modes of quartz using Quantum Espresso[18] as a function of Si mass between the terrestrial Si isotopic composition to pure ^{30}Si. We found that the

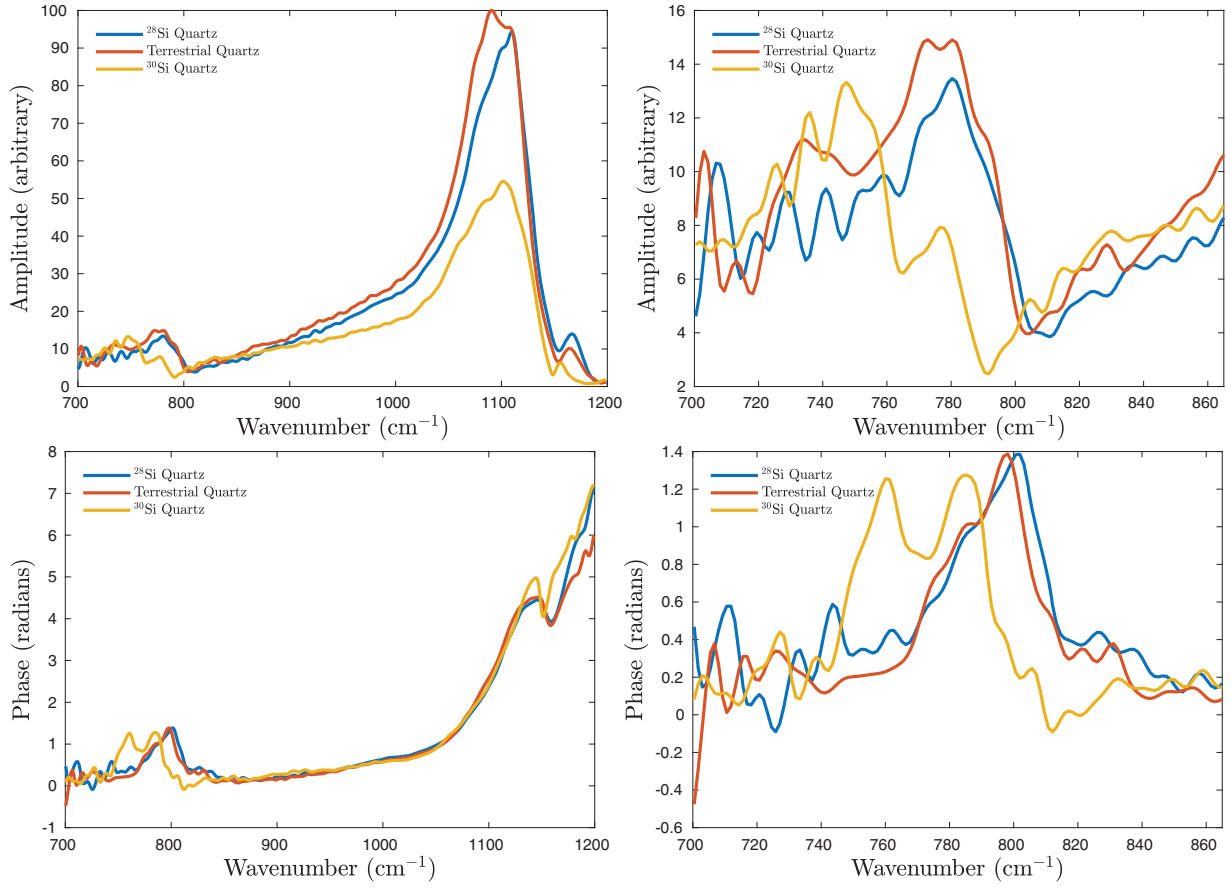

Figure 4. Representative nanoFT-IR spectra of synthetic quartz. Amplitude is on the top left (full spectrum) and top right (detail near 780 cm^{-1}), phase is on the bottom left and bottom right.

vibrational modes of quartz involving Si, as a function of Si mass, are well approximated as a linear function of $\mu^{-1/2}$, where μ is the reduced mass of Si and O (O is assumed to be of terrestrial composition), over the mass range 28–30 amu. Figure 5 shows the fit and residual for one such vibrational mode—the maximum difference between the simplified fit and data is $<0.01\ \mathrm{cm}^{-1}$ in the 28–30 amu range. This approximation makes for simpler error propagation, as described below.

The calculated vibrational modes are well-fit by a linear function of $\mu^{-1/2}$ because the vibrational wavenumber $\tilde{\nu}$ of the Si-O stretch is approximately equal to:

$$\tilde{\nu} = \frac{1}{2\pi c}\sqrt{\frac{k}{\mu}} \quad \mu = \frac{m_{\mathrm{Si}} m_{\mathrm{O}}}{m_{\mathrm{Si}} + m_{\mathrm{O}}} \tag{1}$$

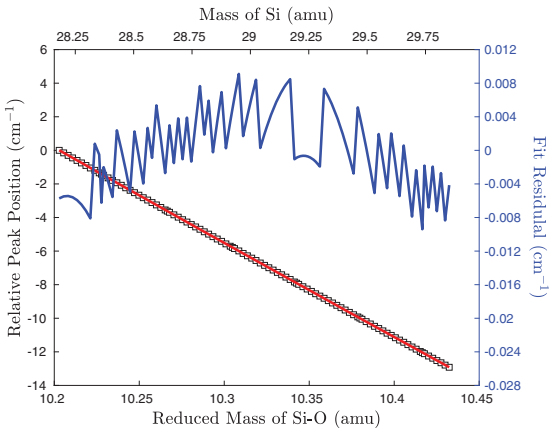

Figrue 5. Calculated peak positions, relative to the terrestrial composition peak position, as a function of mass for a Si–O stretch mode. Black squares are the calculated values using Quantum Espresso, red curve is a fit of this data using a linear function of reduced mass of Si and O (bottom axis) where only the Si mass is varied (top axis). The calculated values minus the fit (the fit residual) is plotted in blue (right axis).

where k is the effective spring constant of the Si–O bond and μ is the reduced mass of the the Si and O atoms. Changing the mass of the Si atom from 28.0855 amu to 30 amu changes the reduced mass, which changes the vibrational frequency of the Si–O stretch. We use this relationship for the general functional form to express our measurements of the wavenumber $\tilde{\nu}$ as a function of the Si–O reduced mass:

$$\tilde{\nu} = \frac{a}{\sqrt{\mu}} + b \tag{2}$$

Figure 6 shows our measurements of $\tilde{\nu}$ as a function of the reduced mass of Si–O, with O = 16.00 amu (terrestrial) and Si = 28.00, 28.11 (terrestrial), 29.93 amu for the three synthesized quartz samples, along with the fitted function.

We solve μ using Eq. 2 and calculate the uncertainty of the reduced mass, σ_μ, using propagation of errors:

$$\sigma_\mu = \sqrt{\left(\frac{\partial\mu}{\partial a}\right)^2\sigma_a^2 + \left(\frac{\partial\mu}{\partial b}\right)^2\sigma_b^2 + \left(\frac{\partial\mu}{\partial\tilde{\nu}}\right)^2\sigma_{\tilde{\nu}}^2 + 2\frac{\partial\mu}{\partial a}\frac{\partial\mu}{\partial b}\sigma_{ab}} \tag{3}$$

where:

$$\frac{\partial\mu}{\partial a} = \frac{-2\tilde{\nu}}{(a\tilde{\nu}+b)^3} \tag{4}$$

$$\frac{\partial\mu}{\partial b} = \frac{-2}{(a\tilde{\nu}+b)^3} \tag{5}$$

$$\frac{\partial\mu}{\partial\tilde{\nu}} = \frac{-2a}{(a\tilde{\nu}+b)^3} \tag{6}$$

This function expresses the uncertainty in mass σ_μ (and, therefore, the uncertainty in isotopic composition) as a function of the fit parameters a and b and their variances (σ_a^2, σ_b^2) and covariance (σ_{ab}), and the uncertainty in the determination of the peak position $\sigma_{\tilde{\nu}}$. Plots of σ_μ as a

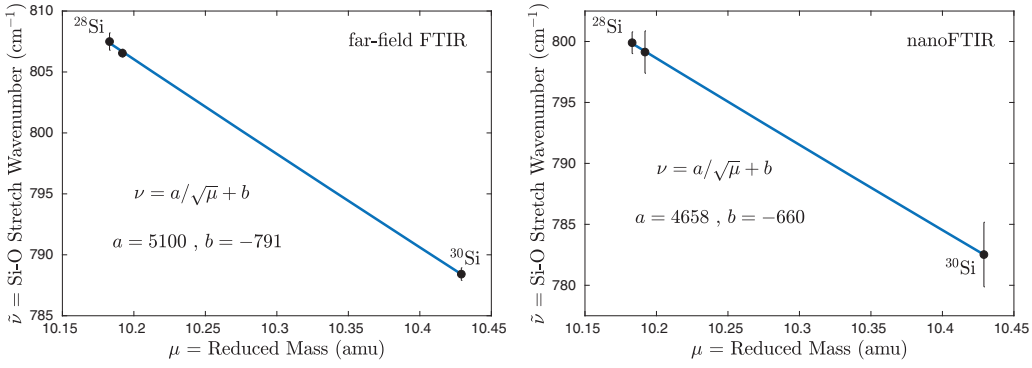

Figure 6. Measured position of IR feature as a function of the reduced mass of the sample. Error bars are the standard deviation of individual measurements.

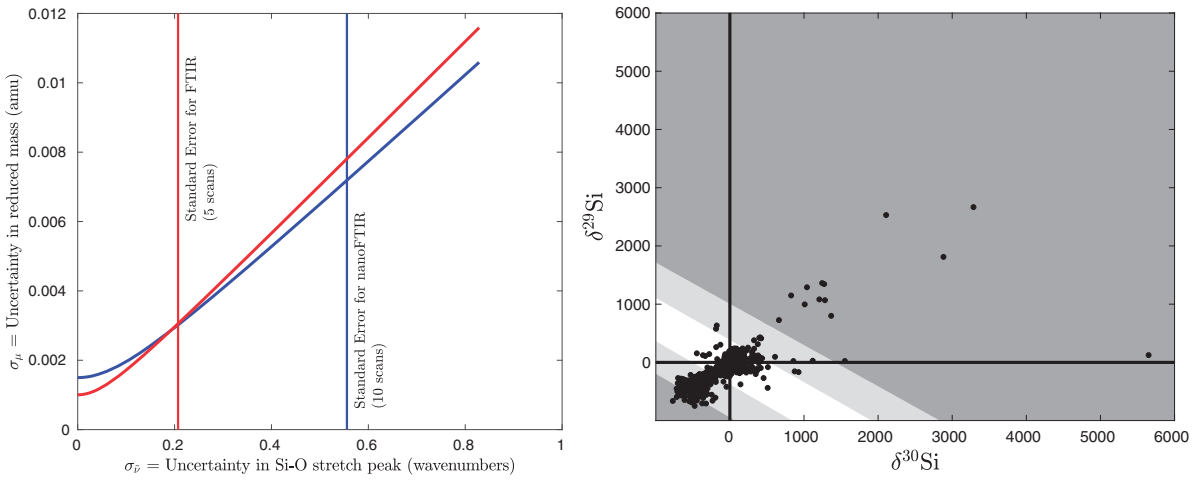

Figure 7. Left: Detectable anomaly by far-field and nanoFT-IR. Right: 1σ detectable presolar SiC grains with far-field FT-IR (five scans, light gray and dark gray) and nanoFT-IR (10 scans, dark gray).

function of $\sigma_{\tilde{\nu}}$, for the fit parameters *a* and *b* calculated for far-field and nanoFT-IR, are shown in Fig. 7.

Isotope ratios in geochemistry and cosmochemistry are typically expressed as "delta values", defined for Si isotopes as:

$$\delta^{29,30}\mathrm{Si} = \left(\frac{\left(^{29,30}\mathrm{Si}/^{28}\mathrm{Si}\right)_{\mathrm{sample}}}{\left(^{29,30}\mathrm{Si}/^{28}\mathrm{Si}\right)_{\mathrm{standard}}} - 1 \right) 1000 \qquad (7)$$

Finally, we use our calculated σ_{μ} for both far-field and near-field IR spectroscopy to determine the minimum detectable δ^{29}Si and δ^{30}Si anomaly. For a given pair of δ^{29}Si and δ^{30}Si values, we calculated the atomic fraction of ^{28}Si, ^{29}Si, and ^{30}Si, and assumed that the three O isotopes had the terrestrial fractions. For each of the nine possible ^{X}Si–^{Y}O combinations, we calculated the product of the ^{X}Si and ^{Y}O fractions and nine reduced masses (Eq. 1). We calculated the dot product of these nine values, which gave us a reduced mass value for each δ^{29}Si, δ^{30}Si pair: $\mu(\delta^{29}\mathrm{Si}, \delta^{30}\mathrm{Si})$. For each location (pixel) on a plot of δ^{29}Si versus δ^{30}Si (Fig. 7), we first colored all pixels white. Then, for each pixel, if $\mu(\delta^{29}\mathrm{Si}, \delta^{30}\mathrm{Si}) - \mu(0,0) > 0.0028$ amu ($= \sigma_{\mu,\mathrm{FTIR}}$), we colored the pixel light gray. Finally, if $\mu(\delta^{29}\mathrm{Si}, \delta^{30}\mathrm{Si}) - \mu(0,0) > 0.0072$ amu ($= \sigma_{\mu,\mathrm{nanoFTIR}}$), we colored the pixel dark gray.

The detectable anomalies for far-field and near-field FT-IR are shown in Fig. 7. We compare these detectable anomalies with Si isotopes measured in presolar SiC grains, which have been studied much more extensively than presolar SiO_2. The detectable anomalies are small enough to identify SiC grains of type X (very low $\delta^{29,30}$Si values, thought to originate from supernovae) and type C (very high $\delta^{29,30}$Si values, also thought to originate from supernovae).[1] The number of detectable grains by nanoFT-IR appears to be smaller (Fig. 7) because the signal-to-noise ratio is lower than far-field FT-IR. However, nanoFT-IR is capable of detecting very small supernova grains, possibly as small as 30 nm. This spatial resolution is better than the NanoSIMS, the SIMS instrument most commonly employed to search for presolar grains in situ. It is possible that more supernova grains can be detected in this very small size range, which are closer to the theoretical sizes predicted for supernova dust (e.g., Bianchi and Schneider[19]). The smaller anomalies seen in the Si isotopic composition of grains that formed from AGB stars are mostly not accessible by IR spectroscopy. However, it is often desirable to screen for presolar SiC X or C grains in order to study the astrophysics of supernovae (e.g., Liu et al.[20]), so such a capability would be very useful for statistical studies of a supernova grains. The Si isotopic compositions of presolar silica grains from supernovae have not yet been measured. Identification of small supernova grains using nondestructive techniques, such as the technique presented here, should allow for new studies to be carried out on relatively understudied population of presolar grains such as presolar silica.

Conclusion

We have demonstrated that IR spectroscopy, both near-field and far-field, can be used to nondestructively identify presolar grains. The traditional method of identifying presolar grains by secondary ion mass spectrometry consumes part of the grains and creates an ion-damaged layer that compromises structural analyses. Our proposed method using IR spectroscopy can nondestructively identify supernova grains as small as 30 nm (exceeding the spatial resolution of the NanoSIMS) for further study.

Presolar grains are present in meteorite matrices at the part-per-million levels, so it is not feasible to acquire 10 min analyses on millions of sub-μm grains to identify supernova grains. A better approach would be to acquire maps over, for example, a mm-sized matrix area of a primitive chondrite (prepared as a polished thin section) at a few diagnostic wavenumbers around the major Si–O stretch of quartz ($\sim$1100 cm^{-1}) to identify small quartz grains. After the quartz grains have been identified, then just those grains can be measured around the 780 cm^{-1} feature to identify the isotope anomaly. This could be done with tunable quantum cascade lasers in the appropriate frequency range, which can be attached as modules on the NeaSpec nanoFT-IR system.

Conflict of Interest

The authors report there are no conflicts of interest.

Funding

This work was supported by NASA Grant NNX14AG25G to RCO and NASA grant NNX15AJ25G to MJK. This is Lunar and Planetary Institute Contribution Number 2148.

ORCID iD

Ryan C. Ogliore https://orcid.org/0000-0001-8165-6252

References

1. E. Zinner. "Presolar Grains". Treatise on Geochemistry. 2003. 1: 711.
2. S. Messenger, L.P. Keller, F.J. Stadermann, et al. "Samples of Stars Beyond the Solar System: Silicate Grains in Interplanetary Dust". Science. 2003. 300(5616): 105–108.
3. S. Amari, R.S. Lewis, E. Anders. "Interstellar Grains in Meteorites: I. Isolation of Sic, Graphite and Diamond; Size Distributions of Sic and Graphite". Geochim. Cosmochim. Acta. 1994. 58(1): 459–470.
4. C. Floss, F.J. Stadermann. "Presolar Silicate and Oxide Abundances and Compositions in the Ungrouped Carbonaceous Chondrite Adelaide and the K Chondrite Kakangari: the Effects of Secondary Processing". Meteoritics Planet. Sci. 2012. 47(6): 992–1009.
5. T. Daulton, T. Bernatowicz, R. Lewis, et al. "Polytype Distribution in Circumstellar Silicon Carbide". Science. 2002. 296(5574): 1852–1855.
6. N. Liu, A. Steele, L.R. Nittler, et al. "Coordinated EDX and Micro-Raman Analysis of Presolar Silicon Carbide: A Novel, Nondestructive Method to Identify Rare Subgroup Sic". Meteoritics Planet. Sci. 2017. 52(12): 2550–2569.
7. R.K. Sato, P.F. McMillan PF. "An Infrared and Raman Study of the Isotopic Species of. Alpha.-Quartz". J. Phys. Chem. 1987. 91(13): 3494–3498.
8. P. Haenecour, X. Zhao, C. Floss, et al. "First Laboratory Observation of Silica Grains from Core Collapse Supernovae". Astrophys. J. Lett. 2013. 768(1): L17.
9. J. Rho, T. Kozasa, W. Reach, et al. "Freshly Formed Dust in the Cassiopeia a Supernova Remnant as Revealed by the Spitzer Space Telescope". Astrophys. J. 2008. 673(1): 271.
10. M.J. Krawczynski, T.L. Grove. "Experimental Investigation of the Influence of Oxygen Fugacity on the Source Depths for High Titanium Lunar Ultramafic Magmas". Geochim. Cosmochim. Acta. 2012. 79: 1–19.
11. V. Swamy, S.K. Saxena, B. Sundman, et al. "A Thermodynamic Assessment of Silica Phase Diagram". J. Geophys. Res. 1994. 99(B6): 11787–11794.
12. J.J. Sahlin, N.A. Peppas. "Near-Field FTIR Imaging: A Technique for Enhancing Spatial Resolution in FTIR Microscopy". J. Appl. Polymer Sci. 1997. 63(1): 103–110.
13. G. Dominguez, A.S. McLeod, Z. Gainsforth, et al. "Nanoscale Infrared Spectroscopy as a Non-Destructive Probe of Extraterrestrial Samples". Nat. Commun. 2014. 5: 5445.
14. P. McMillan P. "Structural Studies of Silicate Glasses and Melts-Applications and Limitations of Raman Spectroscopy". Am. Mineral. 1984. 69(7–8): 622–644.
15. W.H. Press, S.A. Teukolsky. "Savitzky–Golay Smoothing Filters". Comput. Phys. 1990. 4(6): 669–672.
16. R.K. Vincent, G.R. Hunt. "Infrared Reflectance from Mat Surfaces". Appl. Opt. 1968. 7(1): 53–59.
17. P.M.A. Sherwood. Vibrational spectroscopy of solids. 1. Cambridge: CUP Archive, 1972.
18. P. Giannozzi, S. Baroni, N. Bonini, et al. "Quantum Espresso: A Modular and Open-Source Software Project for Quantum Simulations of Materials". J. Phys. Condens. Matter. 2009. 21(39): 395502.
19. S. Bianchi, R. Schneider. "Dust Formation and Survival in Supernova Ejecta". Mon. Not. Roy. Astron. Soc. 2007. 378(3): 973–982.
20. N. Liu, A. Steele, L.R. Nittler, et al. "A Novel and Non-Destructive Method to Identify Rare Type Presolar SiC: Coordinated EDX and Micro-Raman Analysis". LPI Contributions. 2016. 1921: 6094.